X-IronPort-AV: i="4.13,168,1167638400";
d="scan'208"; a="16857109:sNHT28554320"
X-IronPort-AV: i="4.13,168,1167638400";
d="scan'208"; a="16857104:sNHT26752820"
Date: Wed, 10 Jan 2007 09:31:54 -0800 (PST)
From: sirsi@library-r.llnl.gov
To: anderson123@llnl.gov, johnson69@llnl.gov, townsel1@llnl.gov,
illaccts@mail.llnl.gov
Subject: Electronic 1119 Photocopy/ILL Order

Employee Name: Lin, Jung-fu
Employee Number: 007549
LCode: L-415
Phone: 4-4157
Email: lin24@llnl.gov
Account Number: 5283-51

Title: High Pressure Research
Volume: 17
Pages: 57-75
Journal Publication Year: 2000
Article Title: Pressure-induced phase transitions in gypsum
Article Authors: Eugene Huang et al.
Need by Date: ASAP
Notes: A pdf copy is preferred.
Send circulating copy: No
Photocopy item: Yes
Obtain through ILL: Yes
Purchase item: Yes

High Pressure Research, 2000, Vol. 17, pp. 57–75
Reprints available directly from the publisher
Photocopying permitted by license only

PRESSURE-INDUCED PHASE TRANSITIONS IN GYPSUM

EUGENE HUANG[a,*], JI-AN XU[a], JUNG-FU LIN[b] and JING-ZHU HU[c]

[a]*Institute of Earth Sciences, Academia Sinica, P.O. Box 1-55, Nankang, Taipei, ROC;* [b]*Dept. Geophysical Sciences, University of Chicago, Chicago, IL, 60637, USA;* [c]*Geophysical Laboratory, Carnegie Institute of Washington, Washington D.C., 20015, USA*

(Received 5 April 1999; In final form 6 August 1999)

We report high-pressure Raman scattering spectroscopy and energy dispersive X-ray diffraction investigations on gypsum, $CaSO_4 \cdot 2H_2O$, at room temperature in a diamond cell. With increasing pressure, measurements indicate that $CaSO_4 \cdot 2H_2O$ undergoes two stages of crystalline-state phase transitions at 5 and 9 GPa, and then converts to a disordered phase above 11 GPa. The structures of the three high-pressure phases of gypsum have not been determined yet. These phases are tentatively named as "*post-gypsum-I*" (PG-I), "*post-gypsum-II*" (PG-II) and "*disordered*" according to the sequence of their appearance with pressure.

Gypsum shows anisotropic compressibility along three crystallographic axes with $b > c > a$ below 5 GPa. The difference in the behavior of the two OH stretching modes in gypsum is attributed to the different reduction rate in the hydrogen bonding distances by the anisotropic axial compressibility.

Keywords: Gypsum; disordered; OH stretching modes; anisotropic compressibility

1. INTRODUCTION

Hydrous phases are important mineral species for the investigation of the dynamics in the Earth's mantle. For instance, dehydration, amorphization and other phase transitions in hydrous minerals are linked to the mechanisms of the generation of deep-focus earthquakes [1, 2]. In the past few years, we have put much effort into investigating

*Corresponding author. Fax: 886-2-2783-9871, e-mail: eugene@earth.sinica.edu.tw

the high-pressure behavior of compounds in the $Al_2O_3-H_2O$ system in order to reveal the effect of OH bonding on the lattice dynamics of the hydrous phases in general [3, 4]. Recently, in an attempt to measure the solubility of gypsum, $CaSO_4 \cdot 2H_2O$, in a diamond cell, we found that the solubility of gypsum in water increases with pressure up to 1.1 GPa, where water converts to one of its crystalline phases, ice VI. In order to better quantify the role that OH groups play in gypsum under pressure, we have further carried out a series of Raman spectroscopic investigations of gypsum in different pressure media. Several stages of phase transitions were then recognized in $CaSO_4 \cdot 2H_2O$ based on the change in the patterns of the Raman vibrational modes. Thus we have undertaken *in situ* X-ray diffraction experiments to reveal the structural identity of the phases which may occur in gypsum under high pressure. The results might have important implications for understanding the effect of pressure on the behaviors of the OH groups in the hosting hydrous phases in general.

2. EXPERIMENTAL METHODS AND RESULTS

2.1. Raman Spectroscopy

Natural single-crystal of gypsum ($CaSO_4 \cdot 2H_2O$) was used as the starting material. The observed Raman spectrum at the ambient condition is in excellent agreement with that reported by Berenblut *et al.* [5]. A piston-cylinder type diamond anvil cell was used as pressure generator. The diameter of the culet face of the diamonds was 350 μm. A 250 μm-thick disk of T301 stainless steel was used as a gasket. The gasket was indented between the diamond anvils and a hole of 150 μm was drilled to serve as the sample chamber. The chamber was loaded with the sample (single-crystal of about 80 μm × 80 μm × 25 μm in size) and with either 4 : 1 methanol–ethanol mixture or liquid argon as a pressure transmitter. The ruby fluorescence method was used for pressure measurements [6]. In each pressure measurement, we measured more than three ruby grains to estimate the pressure distribution of the compressed sample. We used a Renishaw 2000 Raman spectrometer and an Ar-ion laser beam (514.5 nm) as excitation source. The laser light (about 5 μm in diameter) was focused on the sample in the diamond cell and the back-scattered Raman signal was collected and

analyzed with a CCD detector. The power for the laser source used was 100 to 500 mW and recording time of each Raman spectrum was 200 to 600 seconds. On a few occasions, a longer period of time up to a maximum of 1800 seconds was required to obtain better statistics for the results. Pressure was also measured after each Raman spectra was collected. Although several ruby chips were measured, only the ruby signal at which the Raman spectrum of the sample was collected was taken as the pressure reading to avoid pressure gradient which became significant when the pressure medium was solidified.

Two different pressure transmitting media, *i.e.*, 4 : 1 mixture of methanol–ethanol solution and liquid argon, were used in the experiments. The results in using methanol–ethanol solution and argon as pressure medium are essentially the same. We will only report the results using argon as pressure medium because this run was carried out to much higher pressure. In the experiments with argon as pressure transmitting medium, the pressure was gradually increased up to 24 GPa and then decreased to the ambient condition. Therefore, the Raman spectra of the sample in both the loading and unloading processes were collected.

The wavenumber range of the Raman spectrum covered is divided into two parts. The low-wavenumber (LW) region ranges from 200 to 1300 cm^{-1}. The high-wavenumber (HW) region ranges from 2800 to 3700 cm^{-1}. At high pressure, six Raman modes (listed as ν_1 to ν_6 in Tab. I) showed up in the LW region. The most intense mode (*i.e.*, ν_5 at $\sim 1000\ cm^{-1}$), although it shows discontinuities and mode splittings with pressure, can be tracked up to 24 GPa (Fig. 1). The other LW modes were relatively weak and were not observed above 20 GPa. The modes in the HW regions (ν_7 and ν_8 in Tab. I) showed a drastic change to three new modes between 4 and 5 GPa and the new modes were no longer observed above 8 GPa (Fig. 2). The variations of the wavenumber of each Raman mode of the sample with pressure are listed in Table I. The wavenumber *versus* pressure plots are shown in Figures 3 and 4 for various modes in the LW and HW region, respectively.

2.2. X-ray Diffraction

The natural single-crystal of gypsum used in the present Raman spectroscopic study was ground to powder with an average grain size of 2 μm and then used as the starting material in the diffraction

TABLE I Variation of the wavenumber (in cm^{-1}) of various Raman-active vibrational modes of gypsum with pressure

$P(GPa)$	ν_1	ν_{21}	ν_2	ν_{31}	ν_3	ν_4	ν_{51}	ν_5	ν_{511}	ν_6	ν_{61}	ν_{611}	ν_{71}	ν_7	ν_8
0	416	–	495	–	619	672	–	1009	–	1141	–	–	–	3404	3492
2.04	420	–	504	604	625	680	–	1020	–	1155	–	–	–	3400	3465
2.19	421	–	505	607	625	682	–	1022	–	1157	–	–	–	3399	3460
3.09	422	–	507	609	627	682	–	1026	–	1164	–	–	–	3397	3456
3.54	423	–	509	612	629	684	–	1028	–	1164	–	–	–	3397	3448
4.01	423	–	509	611	628	683	–	1030	–	1167	–	–	–	3394	3444
4.60	420	–	520	–	625	689	1026	1034	–	1176	1156	–	3257	3312	3399
5.51	416	–	523	602	624	–	1018	1027	–	1178	1157	–	3242	3293	3386
6.70	420	–	528	–	627	691	1022	1032	–	1186	1161	–	3217	3261	3342
8.12	426	508	531	–	630	696	1027	1037	–	1192	1168	–	3183	3220	3306
8.94	433	510	533	–	626	–	1027	1034	–	1185	–	1112	–	–	–
10.51	437	515	541	–	626	–	1026	1040	–	1191	–	1116	–	–	–
11.37	436	520	549	608	632	–	1033	1043	–	1194	–	1119	–	–	–
12.68	438	521	551	610	633	–	1033	1042	1050	1194	–	1119	–	–	–
14.15	445	526	553	615	634	–	1036	1044	1056	–	–	1127	–	–	–
15.19	448	530	–	616	639	–	1040	1049	1061	–	–	1129	–	–	–
15.92	450	531	–	–	–	–	1040	1050	1062	–	–	1130	–	–	–
18.02	455	535	–	–	–	–	1044	1055	1070	–	–	1137	–	–	–
18.51	458	536	–	–	–	–	1045	1058	1075	–	–	1141	–	–	–
18.96	458	542	–	–	–	–	1042	1060	1076	–	–	1148	–	–	–
19.72	461	545	–	–	–	–	1047	1063	1081	–	–	1149	–	–	–
20.99	–	–	–	–	–	–	1055	1068	1085	–	–	1156	–	–	–
21.48	–	–	–	–	–	–	1055	1068	1083	–	–	–	–	–	–
22.45	–	–	–	–	–	–	1057	1073	1091	–	–	–	–	–	–
23.47	–	–	–	–	–	–	1069	1076	1094	–	–	–	–	–	–
21.30	–	–	–	–	–	–	–	1058	1076	–	–	–	–	–	–
17.60	–	–	–	–	–	–	–	1051	1067	–	–	–	–	–	–
16.04	–	–	–	–	–	–	–	1045	1061	–	–	–	–	–	–
14.34	–	–	–	–	–	–	–	1039	1057	–	–	–	–	–	–
12.29	–	–	–	–	–	–	–	1044	–	–	–	–	–	–	–
9.53	–	–	–	–	–	–	–	1042	–	–	–	–	–	–	–
7.93	–	–	–	–	–	–	–	1036	–	–	–	–	–	–	–
6.44	–	–	–	–	–	–	–	1029	–	–	–	–	–	–	–
5.60	–	–	–	–	–	–	–	1029	–	–	–	–	–	–	–
4.62	–	–	–	–	–	–	–	1024	–	–	–	–	–	–	–
3.94	–	–	–	–	–	–	–	1022	–	–	–	–	–	–	–
1.12	416	–	496	–	622	674	–	1011	–	1140	–	–	–	3405	3486
0	415	–	495	–	620	672	–	1009	–	1137	–	–	–	3406	3484

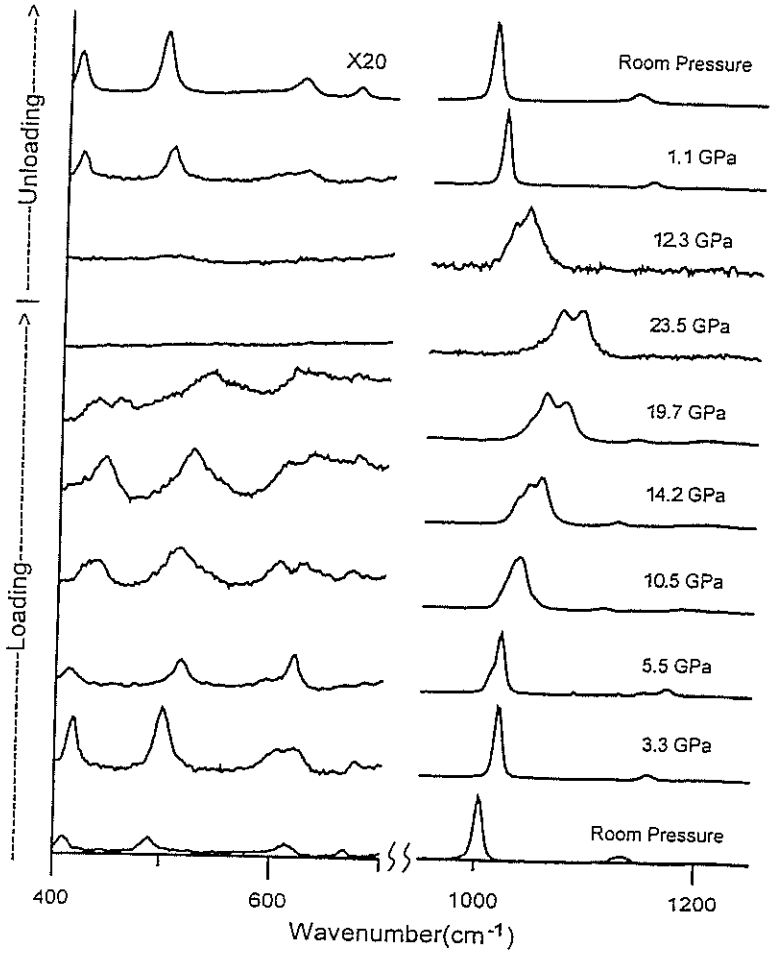

FIGURE 1 A series of Raman spectra of gypsum showing the effect of pressure on the Raman modes in the LW range. The mode at $\sim 1000\,cm^{-1}$ is the most intense Raman mode in gypsum (note the difference in the scale on the right and left side of the spectra). Four stages of changes (between 4.1–4.6 GPa, 8.1–8.9 GPa, 10.5–11.4 GPa and 15.9–18.2 GPa) in the number as well as the wavenumber shift with pressure can be observed in this mode. The gypsum phase was recovered during the unloading process.

experiment. The sample was mechanically mixed with Au powder (Alfa product) which served as pressure calibrant [7]. The mixture was then loaded in the hole (200 μm in diameter) of a T-301 stainless steel gasket

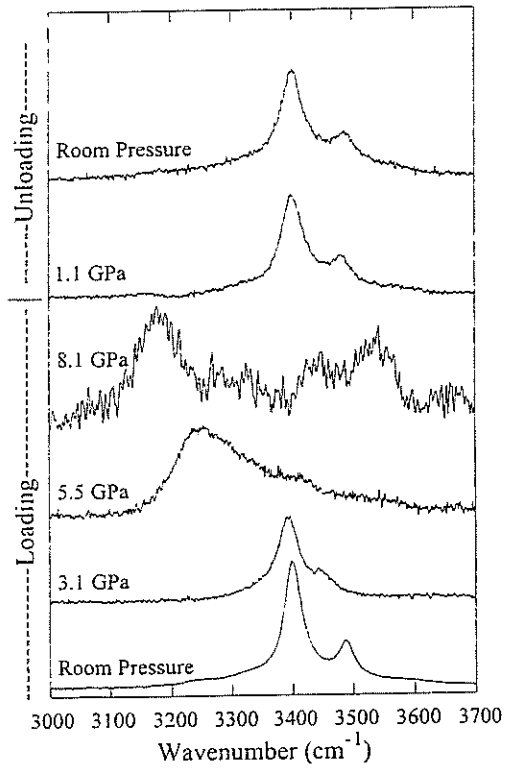

FIGURE 2 Raman spectra of gypsum collected in the HW range showing the changes in the OH stretching modes of gypsum with pressure. The two OH modes convert to 3 modes above 4 GPa and all the modes were no longer observed above 8 GPa. The OH stretching modes of gypsum were not recovered until 1.1 GPa during the unloading process.

and compressed in a diamond cell for high-pressure investigation by the X-ray diffraction method. A 4:1 mixture of methanol–ethanol solution was used as pressure transmitting medium in the experiments.

The X-ray diffraction experiment was carried out at the Brookhaven National Laboratory using the white radiation from the X17C beamline. The size of the synchrotron beam was collimated to $30 \times 30\,\mu m$ and the beam was centered on the sample chamber to reduce the effect of pressure gradient. Pressure was gradually increased up to 15 GPa and then decreased back to the ambient conditions. An energy dispersive X-ray diffraction (EDXRD) pattern was recorded after

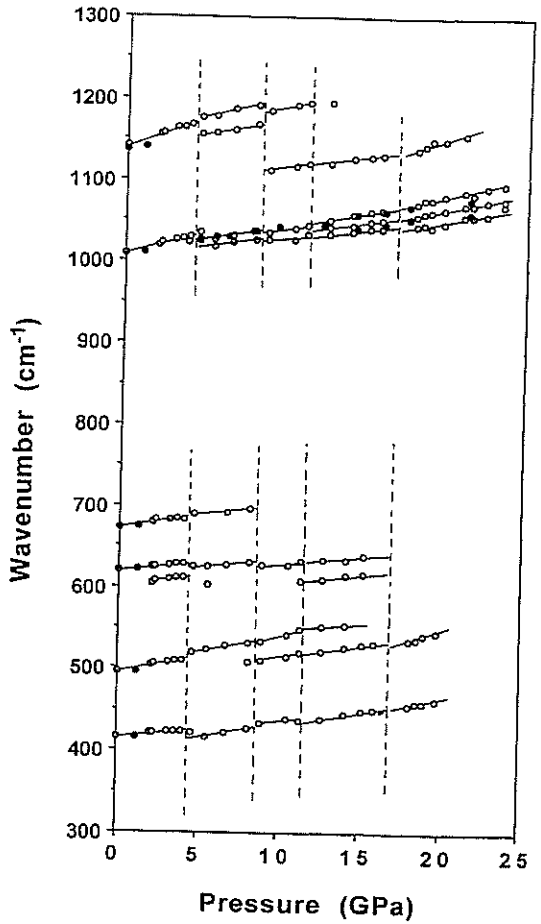

FIGURE 3 The variations of the wavenumber of each Raman mode of $CaSO_4 \cdot 2H_2O$ in the LW range with pressure. Data for the loading process are shown as open circles and unloading process are shown as solid circles. Four stages of change in the slope of the modes as well as the number of modes can be observed. The solid lines are the eye-ball linear fit of the data.

each pressure adjustment with a typical data acquisition time of 5 minutes. The errors associated with the EDXRD method are of the order of 0.2% in d-spacing and the pressure derived from the molar volume of gold has an error of ± 0.5 GPa in the pressure range below 20 GPa.

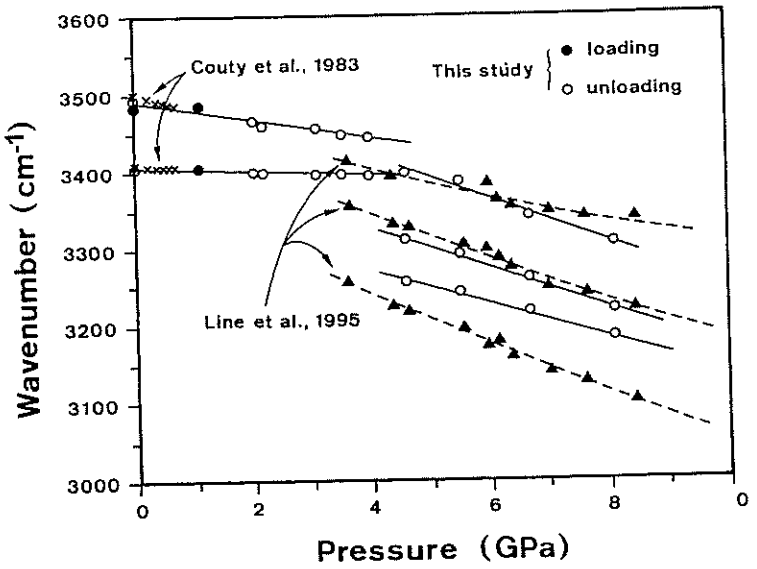

FIGURE 4 The variation of the wavenumber *versus* pressure for the OH stretching modes of $CaSO_4 \cdot 2H_2O$. Open circles and solid circles are obtained in this study during the loading and unloading processes, respectively. The data obtained by Couty *et al.* [9] are shown as crosses which do not significantly deviate from our measurements. Three modes replacing the original OH modes show up above 5 GPa. The variation trends of these modes with pressure are similar to those of the ice VII shown as dashed curves. The data for ice-VII (solid triangles and dashed curves) and from Lin *et al.* [3].

A series of EDXRD patterns which summarize the structural changes in gypsum are shown in Figure 5. With the increase of pressure, $CaSO_4 \cdot 2H_2O$ shows two consecutive crystalline-state phase changes at about 5 and 9 GPa. The diffraction peaks of $CaSO_4 \cdot 2H_2O$ can hardly be recognized when the sample was compressed to 11 GPa at which only a broad hump was observed among the diffraction peaks of gold powder. The diffraction patterns of the sample above 11 GPa did not show any obvious change up to the maximum pressure attempted of 15 GPa. During the unloading process, the general shape of the diffraction pattern remained until 3 GPa where the conversion to a crystalline phase took place. This crystalline phase persisted to room pressure without undergoing further phase transition. The variations of the d-spacing of the diffraction peaks for the various phases as a function of pressure are plotted in Figure 6 from which the pressure at

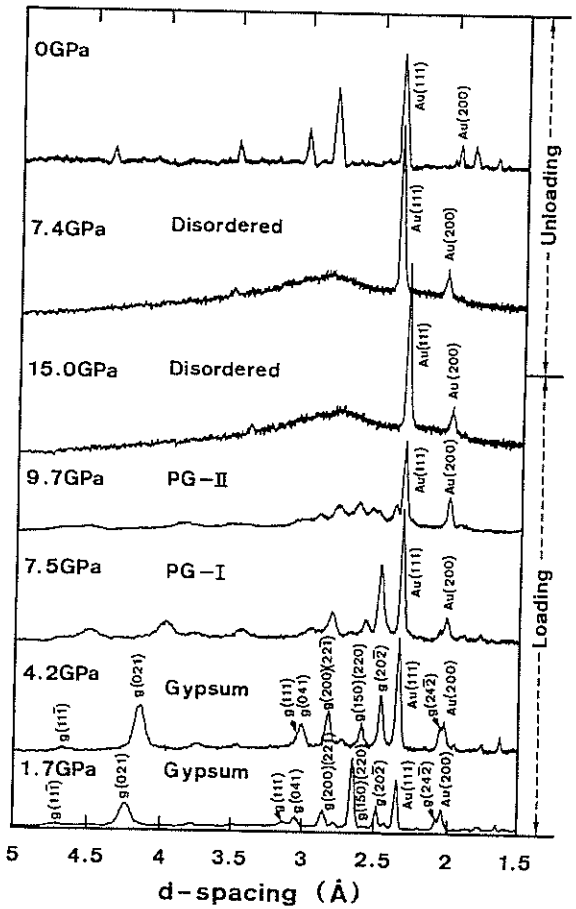

FIGURE 5 A series of EDXRD patterns showing the sequences of phase transitions in gypsum during the loading and unloading processes. Gypsum shows two stages of crystalline state phase transitions to its post-gypsum-I (PG-I at 5 GPa) and post-gypsum-II (PG-II, at 8 GPa) phase which further converts to a disordered phase (at 11 GPa) during the loading process. The disordered phase persists during the unloading process until 3 GPa where the conversion to the PG-I phase takes place.

which each phase transition occurs can be pinned down more accurately. The lattice parameters (a, b and c) and the molar volume of gypsum can be calculated from the various diffraction peaks shown in Figure 6. Table II lists the compression data of gypsum up to 5 GPa.

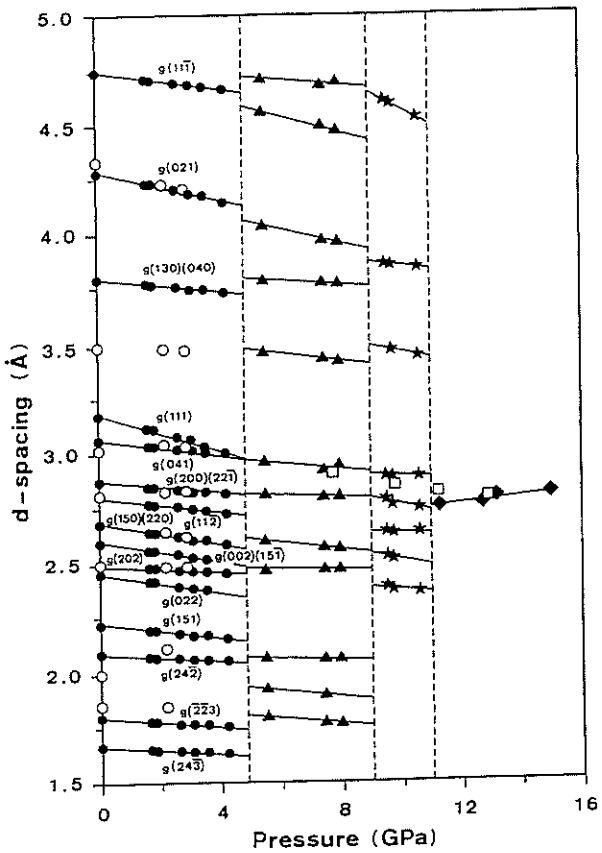

FIGURE 6 The variations of d-spacing of each diffraction peak in various phases of $CaSO_4 \cdot 2H_2O$ as a function of pressure. The solid and open symbols represent the data obtained during the loading and unloading processes, respectively. The pressure at which each phase transition occurs can be pinned down more accurately in this plot. Gypsum (solid circle) remains stable up to 4.3 GPa and then converts to PG-I phase at 5.5 GPa. The PG-I phase (triangle) converts to PG-II phase (star) between 7.5 GPa and 9.7 GPa. The diffraction peaks in the crystalline state disappear above 11 GPa where disordering (solid square) takes place. The disordered phase (open square) persists during the unloading process at least to 7.4 GPa and then converts to PG-I phase (open circle) below 3 GPa.

The calculation was based on the program reported by Novak and Coville [8]. The variations of three lattice parameters and molar volume of gypsum with pressure are plotted and shown in Figure 7.

TABLE II The compression data of gypsum below 5 GPa

Pressure (GPa)	*a (Å)*	*b (Å)*	*c (Å)*	*β*	*Molar volume (Å³)*
0	6.280(2)	15.201(8)	5.667(2)	113.95(5)	495.1(0.6)
1.66	6.254(16)	15.055(47)	4.626(14)	114.58(29)	482.4(3.4)
1.85	6.253(16)	15.042(47)	5.622(14)	114.61(29)	481.4(3.9)
2.62	6.231(20)	14.986(59)	5.593(18)	114.91(36)	473.7(4.9)
3.11	6.218(22)	14.920(64)	5.579(19)	115.12(40)	468.7(5.3)
3.55	6.216(24)	14.909(72)	5.568(22)	115.34(44)	466.2(5.9)
4.23	6.199(28)	14.851(99)	5.557(38)	115.94(70)	460.7(8.3)

The numbers in the parenthesis indicate the error, for instance, (16) means the error is ±0.016; and (0.6) means the error is ±0.6.

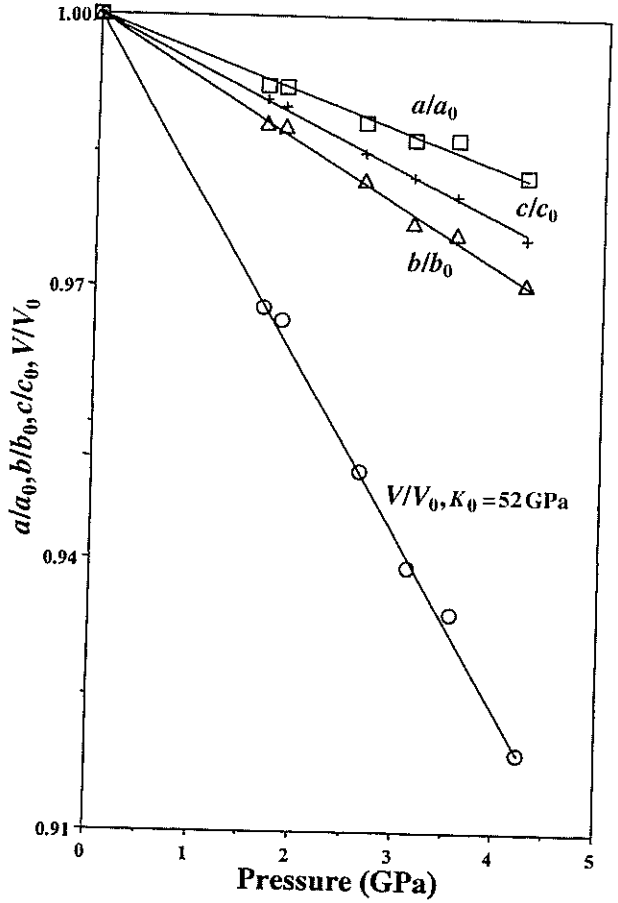

FIGURE 7 The compressibility of the lattice parameters of gypsum up to 5 GPa. The compressibility increases in the order of *a*, *c* and *b*. The compression data was fitted to the equation $P = K(1 - V/V_0)$ and obtained a bulk modulus, *K*, of 52 GPa.

Anisotropic compressibility in three axial directions with *b* being the most compressible and *c* being the most incompressible axis is found in this plot. Since gypsum is relatively compressible, a linear fit of the molar volume compression data yields a bulk modulus value of 52 ± 4 GPa for gypsum.

3. DISCUSSION

3.1. Effect of Pressure on Raman Modes of $CaSO_4 \cdot 2H_2O$

At room pressure, gypsum shows a total of 6 modes in the LW range and 2 modes in the HW range (Figs. 1 and 2). The modes in the LW range correspond to the A_g and B_g modes which are related to the internal bending and stretching modes of SO_4 tetrahedra in the lattice [5]. In our measurements, we did not observe modes other than the bending and stretching modes of the S—O bond in the LW range. The water groups in gypsum show their stretching modes at 3400 and 3500 cm^{-1} but their translational modes at 530 and 557 cm^{-1} [5] were not observed at room pressure. Therefore, the vibrational modes of gypsum observed at high-pressure are all related to the internal vibrations of the sulfate groups and the internal modes of the water groups.

Upon compression, the Raman modes show several stages of discontinuities in the wavenumber *versus* pressure plot (Figs. 3 and 4). The discontinuities occur at between 4.1–4.6 GPa, 8.1–8.9 GPa, 10.5–11.4 GPa and 15.9–18.2 GPa. Additional modes appear when the discontinuities take place. The four stages of discontinuities with the change in the number of modes can be observed more clearly on the most intense mode at around 1100 cm^{-1}. The most drastic change in the pressure-dependent wavenumber shift ($d\nu/dP$) is observed in the two modes in the HW range. The wavenumber of the 3500 cm^{-1} mode decreases more rapidly with pressure while that of the 3400 cm^{-1} mode remains nearly invariant. The difference in the slope of $d\nu/dP$ results in the gradual approach of the two modes at high pressure. The trend in the $d\nu/dP$ of these OH modes is similar to that reported by Couty *et al.* [9] who have studied the pressure effect of the Raman modes of gypsum up to 0.7 GPa. Their reported values of $d\nu/dP$ for 3400 and 3500 cm^{-1} modes are 21 cm^{-1}/GPa and 1 cm^{-1}/GPa, respectively [9],

which are somewhat different from the values of $12\,cm^{-1}$/GPa and $2.5\,cm^{-1}$/GPa determined in this study. However, their data do not show much deviation from our data when plotted in the same diagram (Fig. 4). We believe that our measurements are more representative because our measurements were carried out to much higher pressure. At 4 to 5 GPa, both the ν_7 and ν_8 modes disappeared and three new modes appeared instead. Unfortunately, these new modes were no longer observable above 8 GPa due to the weakness of the signal. During the unloading process, only the modes at $\sim 1000\,cm^{-1}$ are resolved but these modes do not fall on the trends of the modes during the loading process. Instead, they seem to form two separate linear trends which converge at room pressure. Other modes are resolved when the pressure was decreased to less than 2 GPa. In general, the Raman modes of the quenched phase are similar to gypsum but some modes such as ν_5 and ν_6 may also represent the modes of the quenched high-pressure phase. Moreover, the recovered OH bands also suggest that gypsum is the most predominant quenched phase.

3.2. Lattice Distortion in Gypsum

Cole and Lancuchi [10] reported that the water molecules in gypsum form two parallel sheets which are perpendicular to the *b*-axis. The hydrogen atoms lie on the O—O line, forming hydrogen bonds between sulphate and water groups [11]. The two hydrogen sites are termed as external and internal with the latter located between the double layer of oxygens whereas the former lies outside of these layers. The external hydrogen atoms have a hydrogen-bond distance of 2.816 Å and the internal hydrogen atom has a hydrogen-bond distance of 2.896 Å. According to Nakamoto *et al.* [12], the difference in the hydrogen-bond length will result in vibrational modes at 3400 and $3500\,cm^{-1}$ for the H_2O groups. Couty *et al.* [9] interpreted the difference in the pressure-dependent behavior of the OH stretching modes as due to an increase in hydrogen bonding of the less hydrogen-bonded OH (*i.e.*, the $3500\,cm^{-1}$ band). Their interpretation is supported by the quantitative measurements on the compressibility of gypsum in this study.

The compressibility of the three lattice parameters of gypsum below 5 GPa is shown in Figure 7. Gypsum demonstrates anisotropic axial compressibility with *b* being the most compressible axis while *a* being the least compressible axis. In the lattice of gypsum, the SO_4 tetrahedron and H_2O groups both form relatively rigid entities which are less affected during the compression process. The reduction in molar volume at high pressure results mostly from the decrease in the bonding lengths of Ca—O and hydrogen bonds. The decrease in length between the Ca—O bonds may cause the distortion of the SO_4 tetrahedron as detected by the splitting in the Raman modes. The *b*-axis is the most compressible direction where both hydrogen bonds and ionic bonds coexist while ionic bonding predominates along the *a* and *c* directions. As the volume decreases with pressure, the bonding distance between the SO_4 tetrahedron and H_2O groups decreases and therefore results in the enhancement of the hydrogen bond. This results in the lowering of the vibrational frequency of the OH stretching modes in the H_2O groups [13]. The hydrogen bond distance between the oxygen of SO_4 and the internal hydrogen, H(2), decreases drastically while that of the external hydrogen bond remains nearly constant because the most compressed direction is along the *b*-axis. This mechanism accounts for the difference in the pressure dependence of the two OH stretching modes in gypsum.

3.3. Phase Transitions in $CaSO_4 \cdot 2H_2O$

Structural evidence of the phase transition of gypsum is seen in Figures 5 and 6. Gypsum remains stable up to 4.3 GPa and then converts to its high-pressure phase at 5.5 GPa. This high-pressure phase converts to another phase between 8 GPa and 9.5 GPa. The diffraction peaks in the crystalline state persist to 10.3 GPa and then disappear above 11.2 GPa where disordering of the phase takes place. The anomalous behavior that d-spacing increases with pressure above 11 GPa where disordering takes place may be due to the artifact results from the curve fitting program because the peak was too broad to be located. The structures of the two high-pressure phases of gypsum have not been resolved yet. These two phases are tentatively named as "*post-gypsum-I*" (PG-I) and "*post-gypsum-II*" (PG-II) phase according to the sequence of their appearance with increasing pressure.

The pressures at which phase transitions take place in gypsum based on structural evidence were conformable with those observed by the

Raman spectroscopic method. The transition pressures fall in the intervals of (1) from gypsum to PG-I at 4.3 to 4.6 GPa, (2) from PG-I to PG-II at 8.1 to 8.9 GPa, and (3) from PG-II to the disordered phase at 10.5 and 11.2 GPa. Taking into account of the uncertainty in pressure measurements, the pressure values for these transitions are tentatively determined as: from gypsum to PG-I at 4.4 ± 0.3 GPa, from PG-I to PG-II at 8.5 ± 0.5 GPa and PG-II to disordered phase at 10.8 ± 0.4 GPa. Although evidence of another phase transition may be found in Raman modes at 16 to 18 GPa, it lacks the structural identification and, therefore, is not considered in this discussion.

The unloading process was carried out in a more rapid way and only few data could be collected. The disordered phase persists during the unloading process at least to 7.4 GPa and then converts to gypsum below 3 GPa. The diffraction pattern of the quenched sample is in general consistent with the starting material. However, a closer examination of the diffraction peaks of the quenched phase indicates that some of the peaks may be related to the quenched PG-I phase (such as those of 3.5 Å and 2.0 Å, Fig. 6). Although the existence of the quenchable PG-I phase has been ruled out by the Raman spectroscopic observation as discussed above, it is possible that some of the PG-I phase was recovered during the unloading process. The amount of the remaining PG-I phase was only detectable by the X-ray diffraction but was not detected by the Raman spectroscopic method because the OH modes were relatively weak. It is not clear whether PG-II phase has been bypassed while the relatively large pressure adjustment was performed during the unloading process (*i.e.*, from 7.4 GPa to 3 GPa).

3.4. Nature of the Phase Transitions in $CaSO_4 \cdot 2H_2O$

Figure 6 shows that the number of the OH bands of gypsum changes from 2 to 3 modes at 5 GPa. A comparison of the wavenumber of these modes with those of the ice-VII [3] indicates that they behave very similarly (Fig. 4). The OH bands of PG-I phase, especially the ν_7 and ν_8 (Tab. I) are very close to the B_{1g} and E_g mode of ice-VII and the ν_{7I} is systematically higher than the A_g of ice-VII in wavenumber. Therefore, on the basis of Raman observation, one might infer that a pressure-induced dehydration reaction is taking place in gypsum

above 4 GPa where gypsum converts to anhydrite and ice-VII. Nevertheless, none of the phase transitions observed in this study is related to the dehydration of gypsum, because the Raman modes do not agree with those of bassanite and anhydrite which are the candidate de-hydrated phases of gypsum [14]. In addition, no sign of the product phases of dehydration reaction of gypsum was observed in both Raman and X-ray diffraction patterns. We have observed from both Raman and X-ray data that the gypsum phase was recovered during the unloading process. If the dehydration reaction should have taken place, the kinetics of the re-hydrating reaction would have slowed the formation of the original hydrous phase.

The changes in the diffraction patterns during these phase transitions are very drastic and without an intermediate stage. Therefore, the process of transition is very rapid. This implies that the transition is displacive which might be related to the distortion of the lattice instead of reconstructive arrangement of constituting atoms. The Raman modes observed in the LW range are all related to the stretching and bending of the SO_4 groups [5]. The SO_4 group forms a tetrahedron in the lattice of gypsum and has apparently undergone several stages of changes in stretching modes upon compression (Fig. 3). The effect of pressure not only results in the increase in the wavenumber of the S—O stretching modes but also causes the distortion of the SO_4 tetrahedra. For instance, the shortening of the Ca—O bond may cause the degeneracy and splitting of the S—O stretching modes due to the effect of the electrostatic force between Ca and oxygens. The lattice was distorted gradually until at the transition pressure where the rearrangement of the Ca-ions, SO_4 tetrahedra and H_2O molecules causes the structural change of the lattice. The transition from gypsum to PG-I is related to the distortion of the SO_4 tetrahedra and the change in bonding style in H_2O molecules as indicated by the appearance of three ice-VII-like OH modes. Further distortion in the SO_4 tetrahedra and possibly random rearrangements of the Ca-ions, SO_4 tetrahedra and H_2O molecules in the $CaSO_4 \cdot 2H_2O$ lattice result in the transitions to PG-II and finally to the disordered phase. Upon decompression, the conversion from disordered phase to the crystalline phases would normally require sufficient driving force. Therefore, the by-pass of the PG-I and PG-II phases during the unloading process might be caused by the kinetics in the

reshuffling of the constituting molecules to their particular sites. Since the structural identities of the post-gypsum phases are not yet resolved, the transformation mechanism proposed needs to be justified by the results of single-crystal diffraction experiments.

4. SUMMARY

Gypsum was compressed in diamond cells and subjected to Raman spectroscopic study and X-ray diffraction investigation up to 24 GPa and 15 GPa, respectively. The results indicate that:

(1) Both Raman spectroscopy and X-ray diffraction observations support that gypsum undergoes several stages of pressure-induced phase transitions from gypsum to PG-I and then to PG-II and finally to a disordered phase. The pressures phases at which phase transitions take place are: from gypsum to PG-I at 4.4 ± 0.3 GPa, from PG-I to PG-II at 8.5 ± 0.5 GPa and PG-II to disordered phase at 10.8 ± 0.4 GPa.

(2) None of the pressure-induced phase transitions observed is related to the dehydration of gypsum. The structure of the three high-pressure phases of gypsum has not been resolved yet. The disordered phase of $CaSO_4 \cdot 2H_2O$ remains up to 15 GPa and persists during the unloading process until 3 GPa at which it converts back to the gypsum phase.

(3) Anisotropic compressibility along three crystallographic axes of gypsum with $b > c > a$, causes a different reduction rate in the hydrogen bonding distances in two different sites, which results in a difference in the behavior of two OH stretching modes in gypsum below 5 GPa.

(4) The mechanism of the pressure-induced transitions in gypsum is associated with the gradual change in the bonding style of H_2O molecules, the distortion of the SO_4 tetrahedra and the randomization of the constituting molecules in the lattice during compression. Justification of the transition mechanism requires detailed investigation on the structures of the post-gypsum phases.

Acknowledgments

This project was supported by the NSC research grant 85-M001-0202-011 and 86-2613-M213-015. We sincerely grateful to the staff of the Brookhaven National Laboratory for their assistance during our working period at the X17C beamline.

References

[1] Kirby, S. H. (1987). *J. Geophys. Res.*, **92**, 13789.
[2] Meade, C. and Jeanloz, R. (1991). *Science*, **252**, 68.
[3] Lin, J. F., Xu, J. and Huang, E. (1995). *Geol. Soc. China*, **38**, 37.
[4] Huang, E., Li, A., Xu, J., Chen, R. J. and Yamanaka, T. (1996). *Geophys. Res. Lett.*, **23**, 3083.
[5] Berenblut, B. J., Dawson, P. and Wilkinson, G. R. (1971). *Spectrochim. Acta*, **27A**, 1849.
[6] Mao, H. K., Xu, J. and Bell, P. M. (1986). *J. Geophys. Res.*, **91**, 4673.
[7] Heinz, D. L. and Jeanloz, R. (1984). *J. Appl. Phys.*, **55**, 885.
[8] Novak, G. A. and Colville, A. A. (1989). *Am. Mineral.*, **74**, 488.
[9] Couty, R., Velde, B. and Besson, J. M. (1983). *Phys. Chem. Minerals*, **10**, 89.
[10] Cole, W. F. and Lancucki, C. J. (1974). *Acta Crystallogr.*, **30**, 921.
[11] Atoji, M. and Rundle, R. E. (1958). *J. Chem. Phys.*, **29**, 1306.
[12] Nakamoto, K., Margoshes, M. and Rundle, R. E. (1955). *J. Am. Chem. Soc.*, **77**, 6480.
[13] Velde, B. and Martinez, G. (1981). *Am. Mineral.*, **66**, 196.
[14] Huang, E. and Huang, T. (1999). In prep.